A Computational Study of Structural Designs for a Small-diameter Composite Vascular Graft Promoting Tissue Regeneration

Mazin Salaheldin Sirry[1], Peter Zilla[1], Thomas Franz[1,2]*

[1]Cardiovascular Research Unit, Chris Barnard Division of Cardiothoracic Surgery,

[2]Centre for Research in Computational and Applied Mechanics,

University of Cape Town, Cape Town, South Africa

Abbreviated title: Structural designs for tissue regenerative vascular graft

*Corresponding Author:

Cardiovascular Research Unit

Faculty of Health Sciences

University of Cape Town

Private Bag X3

Observatory, 7935

South Africa

Tel: +27 21 406 6418, Fax: +27 21 448 5935

Email address: thomas.franz@uct.ac.za

ABSTRACT

Purpose: The structural integrity and arterial mechanics are important aspects for tissue regenerative vascular grafts with ingrowth permissible porous scaffolds. This paper presents a computational study of structural designs for a small-diameter vascular graft comprising porous polyurethane scaffold and knitted reinforcement mesh using Nitinol and polyurethane wire, respectively.

Methods: Finite element models of the porous scaffold with the knitted mesh as embedded or external reinforcement were generated using validated constitutive models for porous polyurethane and Nitinol. Simulating a luminal pressure of up to 200 mmHg, deformations and stresses were recorded in porous scaffold and knitted mesh.

Results: The models predicted compliance between 1.2 and 15.7 %/100mmHg for the reinforced grafts and 65.1 and 106.4 %/100mmHg for the non-reinforced grafts. For the reinforced grafts, maximum stress was 97.0, 28.2 and 0.055 MPa in Nitinol wire, polyurethane wire and porous polyurethane scaffold, respectively, at 120mmHg. The corresponding maximum strain was 0.27, 5.0 and 22.5%. Stress and strain remained safe in the Nitinol mesh and the porous polyurethane but became critical in the polyurethane mesh between 120 and 200 mmHg. Despite compression due to luminal pressure load, the porous scaffold remained ingrowth permissible for cells, capillaries and arterioles up to 200 mmHg.

Conclusions: The outcomes of this study provided preliminary concepts for the structural designs for a tissue regenerative composite vascular graft towards improved mechanical performance and structural integrity. The implemented modelling approach can be used in the further development and optimization of small-diameter tissue-regenerating vascular grafts.

Keywords: blood vessel; vascular prosthesis; tissue engineering; finite element method; arterial mechanics

1. INTRODUCTION

Atherosclerosis and arteriosclerosis are two common arterial diseases referring to hardening, narrowing and loss of elasticity in major arteries.[26] If not treated, they can lead to ischemia or infarction in the supplied organ.[4] A common treatment for these diseases involves intervention either by using assistive devices to relieve and support the artery as in the balloon angioplasty and endovascular stenting or by replacement or bypassing of the diseased artery with a vascular graft. Arterial and venous grafts (bioprostheses) are preferred to synthetic grafts; however, the long-term success of small and medium calibre bioprostheses is challenged due to the frequently encountered thrombosis, occlusion and aneurism.[8] In addition, other factors such as age, disease or prior usage limit the availability of bioprosthetic grafts for patients requiring redo procedures.[23]

Synthetic grafts have been used as alternatives to bioprostheses. In small diameter synthetic grafts, the long-term patency is limited due to the lack of endothelialisation, anastomotic intimal hyperplasia and surface thrombogenicity.[36] Tissue regeneration provides promising avenue for the development of vascular grafts. This approach, whether aiming at composite implants combining synthetic materials with living cells and tissue or at the complete replacement of initially implanted materials by regenerated tissue, requires ingrowth permitting (i.e. porous) scaffolds with structural properties tailored for implantation in the arterial circulation and mimicking arterial mechanics. The complete healing of the porous vascular graft implies interconnected pores to permit a transmural tissue ingrowth rather than the initially applied trans-anastomotic ingrowth.[24, 36]

Porous polymeric scaffolds typically suffer from a lack of structural stiffness depending on the degree of porosity and tendency to dilate over time owing to the viscoelastic properties of the polymer. Suitable reinforcement of the scaffold is required to improve the structural integrity, in particular when a small wall thickness is desired to minimise the amount of synthetic material to be implanted.

The reinforcement of synthetic vascular grafts has been used extensively for the endovascular repair of abdominal aortic aneurysms[7, 9, 17, 19] whereas this concept is less common in the smaller vasculature.[27, 28, 32] These vascular prostheses comprise PTFE or woven polyester grafts and Nitinol, stainless steel or Co–Cr alloy stents.[7, 27]

The use of Nitinol meshes, braided from 0.05 mm thick wires, has recently been reported as constrictive external reinforcement for saphenous vein grafts in pre-clinical studies,[37, 38] whereas knitted Nitinol mesh variations have been studied in vitro.[30] While textile fabrics were investigated by Yeoman et al.[35] as external reinforcement for small-diameter tissue regenerative polyurethane grafts with well defined interconnected porosity,[2, 6] such knitted meshes may lend themselves as alternative reinforcement structures.

This concept was explored in the current study of a multi-component small-diameter graft promoting vascular tissue regeneration. The primary goal of the study was to investigate structural designs of a porous polyurethane scaffold with knitted reinforcement mesh that provide artery-like mechanics and long-term structural integrity. In order to potentially allow for a complete replacement of the implanted graft with regenerated tissue, polyurethane was considered as material for the knitted mesh in addition to the biostable Nitinol. While time dependent changes in mechanical properties, found in degradable vascular prostheses, were

not considered, the effect of scaffold deformation on cellular and tissue ingrowth spaces was an important aspect in the investigations.

2. MATERIALS AND METHODS

2.1 Geometries

The geometry of the knitted wire mesh was derived from a previous study.[30] In the current study, the inner diameter (ID) of the tubular knitted mesh was adjusted to 3.0 mm (Pro-Engineering Wildfire® 2.0, Parametric Technology Corp., Needham, MA, USA) while maintaining a wire thickness of 0.05 mm (see Fig. 1a). A single loop geometry, which formed a 45° circumferential section, was extracted and imported into Abaqus CAE® 6.8-2 (Dassault Systemes, Providence, RI, USA). The single loop geometry was used to create an assembly of three loops arranged in longitudinally direction of the tubular mesh. Additional partial loops were included at either longitudinal end of the loop assembly to assist with the definition of boundary conditions. In Abaqus CAE®, the loop assembly was complemented with a 45° section of a tubular porous polyurethane (PPU) scaffold with a wall thickness of 0.3 mm such that the loop section simulates an external (EX) or embedded (EM) reinforcement of the PPU scaffold by the knitted mesh, see Fig. 1(b, c). In the EX assembly, the outer diameter (OD) of the PPU scaffold matched the ID of the wire mesh. In the EM assembly, the PPU scaffold was such that the wire mesh was situated radially in the centre between scaffold ID and OD. The ID of the resulting composite graft was 2.40 and 2.84 mm for the EX and EM assembly, respectively. The 45° tubular PPU sections with ID of 2.4 mm (BG2.4) and 2.84 mm (BG2.8), respectively, and wall thickness of 0.3 mm were also used as non-reinforced versions of the EX and EM composite grafts. The partial geometries were assumed to be sufficient for the FE models due to the repetitive structure of the knitted mesh and the axi-symmetry of the tubular PPU scaffold.

2.2 Materials and Constitutive Models

The PPU represented a scaffold structure with well-defined interconnected pores manufactured by a phase inversion and porogen extraction technique[3] using highly regular spherical porogen of a nominal size range of 125-150 μm. The ratio of pore size to porogen size was 1.21 ± 0.07 while the ratio of the size of the interconnecting windows to the pore size was 0.52 ± 0.04.[2] Nitinol and solid polyurethane (PU), respectively, were utilised for the knitted wire mesh.

Abaqus® intrinsic constitutive models were used for all materials. The PPU material was described with a fourth-order isotropic hyperfoam model valid for large strains.[1] Experimentally determined material parameters[35] of the PPU used in this study are summarised in Table 1. Nitinol was represented with Abaqus® shape memory alloy user material with experimentally obtained material parameters[30] as shown in Table 2. For the solid PU, an isotropic linear elastic model was used with an elastic modulus and material density of 570 MPa and 1025 kg/m^3,[34] respectively, and Poisson's ratio of 0.3.[20, 31]

2.3 Finite Element Models

Six FE models were developed from the geometries described above to compare a) PPU grafts without reinforcement, with external wire mesh reinforcement and with embedded wire mesh reinforcement and b) grafts reinforced with Nitinol wire mesh and with PU wire mesh:

- Composite grafts with external Nitinol mesh reinforcement (NIEX) and PU mesh reinforcement (PUEX), respectively, and the associated non-reinforced graft (BG2.4);

- Composite grafts with embedded Nitinol mesh reinforcement (NIEM) and PU mesh reinforcement (PUEM), respectively, and the associated non-reinforced graft (BG2.8).

The wire loops and PPU scaffold were meshed using 8-node linear brick elements. The mesh density was set to ten elements along the wire cross-sectional circumference and six elements in thickness direction of the PPU scaffold, resulting in a total of 20,055 and 28,579 elements for EX and EM assemblies, respectively.

The contact between the PPU section and the wire mesh (for EX models only) and between the individual wire loops (for EX and EM models) was defined as surface-to-surface contact with finite sliding and exponential pressure-overclosure relationship. Master-slave contact pairs were defined between surfaces of individual single loop parts in a sequential order starting from the back partial loop towards the front partial loop, in such a way that loop n acted as a master to loop $n+1$. Additionally, the entire surface of each wire mesh loop was set as slave surface to the abluminal surface of the PPU section which as acted as master surface. The pressure-clearance values were initially set to (0.5 MPa, 0 mm / 0 MPa, 0.005 mm) and adjusted when required to achieve of numerical stability. In the embedded reinforcement models (EX), contact between the wire mesh and the PPU section was governed by the embedded region constraint[1] that was utilized to generate the FE mesh of the wire loops embedded in the PPU section. A frictional tangential behaviour was incorporated in the models based on static-kinetic friction exponential decays. The static friction coefficient for Nitinol-Nitinol contact pairs was set to 0.3[18] whereas the kinetic friction coefficient was assumed to be 0.25. The static friction coefficient for the PPU-PU and PU-PU contact pairs was set to 0.5[5] assuming a kinetic friction coefficient of 0.45. For the PPU-Nitinol contact pairs, a static friction coefficient of 0.2 was used based on the reported polyurethane-metal friction, [22, 25] with an assumed kinetic friction coefficient of 0.18. The decay coefficient was set to 1×10^{-5} for all contact pairs.

The quasi-static analysis was carried out in two steps: 1) Establishment of contact between

the parts, and 2) application of load, a pressure uniformly distributed over the luminal surface of the PPU section. The pressure was increased linearly over entire period of the second step from 0 to 200 mmHg to extend over the physiological blood pressure range. Automatic time incrementation was used to control the time increments in each step. The time period was set to 1.0 with an initial time increment of 0.1. The size of the time increment was automatically adjusted between minimum and maximum values of 1×10^{-12} and 0.025, respectively, to achieve solution convergence.

Based on the circumferentially and longitudinally repetitive pattern of the knitted wire mesh and the axisymmetric geometry of the tubular PPU section, axisymmetric boundary conditions were applied to simulate the physical situation and to compensate for the modelling of partial geometries. With the axisymmetric boundary condition, the model surfaces (labelled with "C" in Fig. 1 b and c) on symmetry planes were restrained from rotation around z- and r-axis and circumferential displacement along the θ-axis, and were allowed to translate along the r- and z-axis and rotate around the θ-axis. With a second set of boundary conditions, all longitudinal cross-sectional surfaces of the models (labelled with "A" in Fig. 1 b and c) were restrained from translation in z-axis and rotation around the r- and θ-axis, while they were allowed to translate along the r- and θ-axis and rotate the z-axis. The omission of the movement of longitudinal cross-sections ("A") in longitudinal direction (z-axis) was adopted from a previous study[30] of knitted wire mesh and was required due to the disassociation of the mesh loops in the external reinforcement models.

The numerical stability and consistency of the models were verified with regard to element type, mesh density, boundary conditions, contact and friction definitions by varying the respective parameters and assessing the effect on the output parameters.

2.4 Data analysis

The maximum principal stress, maximum principal strain and displacement were recorded automatically as Abaqus® output variables. The pressure-diameter relationship and the radial compliance were determined from the pressure applied as load on the luminal surface of the PPU section and the associated radial displacement of that surface captured during the analysis. The pressure-diameter relationship was expressed graphically as curve of pressure versus diameter increase, $\Delta D(P)$, with

$$\Delta D(P) = \frac{D(P) - D_0}{D_0} \tag{1}$$

where $D(P)$ is the diameter at pressure P and D_0 is the diameter at $P = 0$ mmHg.

The radial compliance was calculated from using diastolic and systolic pressure and the associated diameter values,

$$C = \frac{D_2 - D_1}{(P_2 - P_1)D_1} \tag{2}$$

where P_1 and P_2 represent diastolic and systolic blood pressures, and D_1 and D_2 represent the ID of the graft at diastolic and systolic pressure, respectively.

The wall compression was determined by capturing the radial displacement at all corresponding nodes on the luminal and abluminal surfaces of the PPU section.

2.5 Validation

Numerical results were validated using experimental and numerical compliance data from previous studies obtained for the PPU scaffold[35] and the Nitinol wire meshes[30] due to unavailability of graft prototypes comprising the external and embedded reinforcement assemblies. For comparison purposes, additional non-reinforced scaffold model (BG4.0) with ID of 4.0 mm and wall thickness of 7.0 mm was developed utilizing the same procedure and conditions applied for the development of BG2.4 and BG2.8 models.

3. RESULTS

Figure 2 illustrates for all models the pressure-diameter relationship expressed as luminal pressure versus the relative increase in ID of the PPU scaffold. The independent parameter, pressure, was plotted on the vertical axis in line with the convention for pressure-diameter graphs in the medical field. The pressure-diameter change curves of the graft models with external reinforcement displayed a slight increase in the slope at 120 mmHg, see Fig. 2(a). This indicated radial non-linear stiffening although the predicted effect was weak. The Nitinol mesh reinforced model (NIEX) experienced smaller dilation than the graft with PU mesh reinforcement (PUEX). The non-reinforced PPU model (BG2.4) exhibited a considerably increased dilation compared to the reinforced models and terminated prematurely at a pressure of 170 mmHg. The NIEM and PUEM models of embedded reinforcement exhibited a linear pressure-diameter relationship (Fig. 2b). Similar to the externally reinforced models, the graft with embedded Nitinol mesh displayed the least dilation followed by the PU mesh reinforced model, and the non-reinforced PPU model exhibiting excessive dilation and termination at 150 mmHg.

The maximum principal stress and strain are summarized in Table 3 for the different models at pressures of 80, 120 and 200 mmHg, distinguishing between the reinforcement mesh and the PPU scaffold. Stress and strain in the wire mesh were larger in the externally reinforced models compared to their counterparts with embedded reinforcement. The same applied for the PPU scaffold with Nitinol mesh, i.e. larger stress and strain were predicted with external reinforcement compared to embedded reinforcement. However, the opposite was observed for the models with PU wire reinforcement; stress and strain levels in the PPU structure were

lower with external mesh compared to embedded mesh. In the non-reinforced PPU models, stress and strain were between twofold to eightfold higher than the values predicted in the associated reinforced models.

Figures 3 and 4 illustrate the distribution of the maximum principal stress in the deformed models of external and embedded reinforcement, respectively, at 120 mmHg. Due to the large difference in stress values in the wire mesh and the PPU structure, the components were displayed separately providing each structure with its own contour legend. In the NIEX and PUEX models (Fig. 3), stress concentrations were predicted in the heads and intersections of wire loops and on the abluminal surface of the PPU scaffold. The embedded reinforcement models NIEM and PUEM (Fig. 4) coincided with the external reinforcement models with regard to the locations of stress concentration in the wire mesh. However, the stress concentrations in PPU scaffold were predicted in internal elements of the PPU scaffold, but not on the abluminal surface as observed with external mesh. The distribution of the maximum principal strain and locations of strain concentrations in the PPU scaffold and wire mesh, illustrated in Figs. 5 and 6, closely matched that of the maximum principal stress.

The wall compression of the PPU scaffold predicted at 80, 120 and 200 mmHg is illustrated in Fig. 7. Compared to the non-reinforced models, the wall compression was substantially increased in the external reinforcement models and slightly reduced in the embedded reinforcement models. Within each reinforcement system, both the Nitinol-reinforced and PU-reinforced grafts showed nearly equal levels of wall compression.

The radial compliance between 80 and 120 mmHg as the diastolic-systolic pressure range, was predicted to be 7.0, 15.7 and 65.1 %/100mmHg for the models with external Nitinol

mesh, PU mesh and associated non-reinforced scaffold model, and 1.2, 6.4 and 106.4 %/100 mmHg for the grafts with embedded Nitinol mesh and PU mesh as well as the associated non-reinforced scaffold model.

4. DISCUSSION

In this study, potential designs for tissue regenerative vascular composite grafts, comprising a PPU scaffold and reinforcement structure, were investigated using the finite element method. Graft models were developed for external and embedded reinforcement of a PPU scaffold with a knitted mesh of Nitinol and PU wire, respectively, as well as for non-reinforced PPU scaffolds. Physiological loading was simulated in numerical analyses using linearly increasing luminal pressure between 0 and 200 mmHg. The incorporation of the knitted reinforcement mesh considerably improved the mechanical behaviour and structural integrity of the tissue regenerative grafts compared to the non-reinforced porous polyurethane scaffold. The most notable effect of the reinforcement was the prevention of the excessive dilation observed in the non-reinforced porous polyurethane scaffolds.

The incorporation of an external reinforcement reduced the radial compliance of the graft by 89% and 76% for the Nitinol mesh and PU mesh, respectively, compared to the non-reinforced PPU scaffold. A slightly larger reduction of the radial compliance of 99% and 94% was observed for graft reinforcement with the embedded Nitinol mesh and PU mesh, respectively. In particular the compliance values obtained with the external mesh compared well with arterial compliance of 8.0 ± 5.9 %/100mmHg.[29] In spite of the larger diameter of the embedded reinforcement models, the lower compliance values indicated that an embedding of the reinforcing structure in the PPU scaffold increased the radial stiffness of

the graft more than the external application of the mesh support.

The termination of model BG2.4 and BG2.8 when approaching 170 mmHg and 150 mmHg, respectively, was attributed to the numerical instability associated with the excessive dilation experienced by the models indicating structural failure. Generally, the predicted mechanical behaviour of model BG2.4 and BG2.8 revealed high distensibility and structural weakness. Their compliance excessively exceeded the required physiological arterial range of 8.0 ± 5.9 %/100mmHg[29] emphasizing the need for mechanical enhancement.

For both reinforcement types, the Nitinol mesh provided less compliant grafts than the PU mesh. This was expected from the 68-fold difference in the elastic modulus between Nitinol (38,991 MPa) and solid PU (570 MPa). The non-linear stiffening of the external reinforcement models was ascribed to the tightening of the wire loops increasing the structural stiffness of the mesh at higher pressures. This indicated that external reinforcement may provide more arterial like mechanics[15] compared to the embedded mesh that resulted in a linear pressure-diameter curve. A similar non-linear deformation was exhibited by a small-diameter PU vascular graft when reinforced with weft-knitted tubular fabric[33]. However, the differences between embedded and external support were not overly pronounced and did not take into account that an external reinforcement mesh may be attached to the PPU structure by means of an adhesive, e.g. PU layer or fibrin glue. This will affect the mechanics of the mesh towards that of the embedded case since the movement of mesh wire loops will be restrained. Adhesive connection between external mesh support and graft structure is also expected to affect, reduce, the radial graft compliance.

When exposed to a luminal pressure of up to 200 mmHg, assumed as a physiological

maximum, the maximum stress and strain predicted in the PPU scaffold indicated recoverable elastic deformation in the reinforced models. In the Nitinol mesh, both the maximum stress and strain remained uncritical. The stress of 157.9 MPa reached merely 33% of the value associated with the start of austenite-martensite phase transformation, 483 MPa.[30] The maximum strain of 0.43% did not exceed 25% of the recoverable strain of Nitinol of 2% reported for high-cycle loadings.[16] The stress and strain values predicted in the PU wire meshes were compared to tensile properties of PU materials with elastic modulus of 534.4 ± 37.1 MPa[14] similar to that used in this study (570 MPa). The ultimate tensile stress of 31.7 ± 0.6 MPa reported by Grapski and Cooper[14] indicated the likelihood of onset of plastic deformation in the PU wire between 120 and 200 mmHg for both the embedded (PUEM) and the external mesh (PUEX). The maximum strain values predicted in the PUEM and PUEX wire meshes reached merely 2% of the elongation at break of 355.3 ± 18.4 %.[14] Apart from plastic deformation of the graft components, debonding of mesh wire and porous polyurethane may constitute another failure mode in the composite grafts with embedded reinforcement mesh. The consideration of this failure mode was, however, beyond the scope of this study. The embedded region constraint used to represent the embedded mesh in the PPU structure in Abaqus does not provide capabilities to incorporate debonding phenomena in the analysis. As such, a different modelling approach would be needed.

The validation of the PPU scaffold models utilized experimental and numerical data obtained by Yeoman et al.[35] for a non-reinforced PPU graft prototype (ID: 4.0 mm, wall thickness: 7.0 mm). The radial compliance was experimentally measured and numerically predicted to be 16.4 ± 4.6 and 33.9 %/100mmHg, respectively. These values exceeded the compliance predicted for the non-reinforced models in this study (i.e. BG2.4 and BG2.8). The larger wall thickness of the PPU prototype used by Yeoman et al., compared to the non-reinforced

models, was the main factor for the lower compliance in spite of the larger luminal diameter which led to a larger circumferential wall tension at the same luminal pressure.[10, 21] This was confirmed by the decreased compliance predicted for the BG4.0 model (31.17 %/100mmHg) which exhibited identical luminal diameter and wall thickness as the physical prototype. The compliance predicted by model BG4.0 correlated with the numerical compliance of the PPU prototype obtained by Yeoman et al; however, both numerical values exceeded the experimentally determined compliance. Yeoman et al.[35] attributed this overestimation to the potential difference in material/structural properties associated with the preparation of the prototype and the mechanical characterization of the samples used in the development of the material model.

The Nitinol-reinforced models (i.e. NIEX and NIEM) were validated using experimental and numerical compliance data of a Nitinol mesh prototype (ID: 3.35 mm, wire thickness: 0.05 mm). Circumferential tensile tests and volumetric displacement tests indicated a compliance of 5.12±0.8 and 4.55±0.6 %/100mmHg, respectively (unpublished data) whereas the values predicted with an FE model was 2.5 %/100mmHg.[30] Considering that the knitted mesh rested on the abluminal surface of the PPU scaffold in the externally reinforced models, the change in the outer diameter of the PPU scaffold correlated with the change in the inner diameter of the knitted mesh. While the compliance of the models in this study was generally based on the change in inner diameter of the PPU scaffold, the apparent compliance of the knitted mesh may be represented by the change in outer diameter of the PPU scaffold. For the NIEX model featuring the Nitinol mesh, the latter yielded a value of 4.08 %/100mmHg. Due to pressure attenuation through the porous scaffold wall, the transmural pressure that acted on the scaffold-mesh interface was in fact less than the luminal pressure in the PPU scaffold. Hence, the numerical compliance of the Nitinol mesh was somewhat underestimated. Considering in addition the smaller diameter of the knitted mesh in this study (3.0 mm) that

resulted in lower circumferential wall tension compared to the Nitinol mesh of the previous studies (3.35 mm), the data predicted by models in this study showed a reasonable agreement with the experimental data.

The use of a linear elastic constitutive model for the solid polyurethane was assumed satisfactory for this exploratory study. A linear elastic constitutive model has been used for solid PU in an investigation involving the deployment of a balloon-expandable stent[25] when representing a cylindrical PU balloon applying material data of PU ureteral stents.[13]

One crucial aspect in tissue regenerative scaffolds is the dimension of ingrowth spaces. Care has to be taken during the design process to ensure that ingrowth spaces remain sufficiently large under physiological loading so as not to inhibit cellular and tissue ingrowth.[35] Compression of the PPU scaffold due to luminal pressure loading is the principal parameter affecting pore size and ingrowth spaces. Compared to the non-reinforced models, the maximum wall compression observed at 120 mmHg was increased by 211% and 201% when using the Nitinol and PU mesh, respectively, as external reinforcement whereas it was reduced by 44% and 39% with an embedded Nitinol and PU mesh, respectively. In the non-reinforced PPU model, wall compression was primarily governed by transverse contraction of the wall associated with radial dilation and circumferential stretch whereas compression due to the luminal pressure was secondary.[35] The external reinforcement limited the radial dilation, circumferential stretch and associated transverse contraction of the wall. As such, thinning of the wall due to the luminal pressure was the predominant cause of wall compression in this case, having a larger effect than the predominant mechanisms of wall deformation in the non-reinforced models. The embedded reinforcement mesh appeared to combine effects beneficial for limiting the wall compression, namely reduced dilation and

transverse wall contraction with shielding the PPU layer situated ablumenally to the reinforcement from compression due to the luminal pressure.

The average diameter of capillaries ranges from 8 to 10 μm and the diameter of a functional arteriole (including endothelium and smooth muscle) is approximately 30 μm.[11, 12] The PPU scaffold used in this study featured a minimum pore window diameter of approximately 65 μm.[35] Recalling that the maximum wall compression predicted among the different reinforced models was 37.24% (model NIEX at 200 mmHg), the minimum pore window diameter would be reduced to 41 μm. This suggested that the tissue-regenerating characteristic of all grafts was not affected since the scaffold retained permissibility for cellular and tissue ingrowth.

The developed models helped exploring the structural design and mechanical behaviour of the composite vascular graft. The outcomes of this study provided preliminary concepts for the structural optimisation towards improved mechanical performance and structural integrity of such devices. The implemented modelling approach can be used in the further development and optimization of small-diameter tissue-regenerating vascular grafts.

FUNDING SOURCES

CONFLICT OF INTEREST STATEMENT

The authors declare that they do not have conflicts of interest with regard of this manuscript

and the data presented therein.

APPENDIX

Figures with essential colour discrimination: Figs. 3 to 6, in this article are difficult to interpret in black and white. The full colour images can be found in the on-line version.

REFERENCES

[1] Abaqus analysis user's manual. Providence, RI, USA: Abaqus, Dassault Systèmes; 2008.

[2] Bezuidenhout D. Porous polymeric superstructures as in-growth scaffolds for tissue-engineered vascular prostheses [PhD]. Stellenbosch: Stellenbosch University; 2001.

[3] Bezuidenhout D, Davies N, Zilla P. Effect of well defined dodecahedral porosity on inflammation and angiogenesis. ASAIO J. 2002;48(5):465-71.

[4] Crowley LV. An introduction to human disease: Pathology and pathophysiology correlations. 8 ed. Sudbury, MA: Jones & Bartlett Publishers; 2009.

[5] Dammak M, Shirazi-Adl A, Zukor DJ. Analysis of cementless implants using interface nonlinear friction--experimental and finite element studies. J Biomech. 1997;30(2):121-9.

[6] Davies N, Dobner S, Bezuidenhout D, Schmidt C, Beck M, Zisch AH et al. The dosage dependence of VEGF stimulation on scaffold neovascularisation. Biomaterials. 2008;29(26):3531-8.

[7] Desai M, Eaton-Evans J, Hillery C, Bakhshi R, You Z, Lu J et al. AAA stent–grafts: Past problems and future prospects. Ann Biomed Eng. 2010;38(4):1259-75.

[8] Dobrin P, Littooy F, Golan J, Blakeman B, Fareed J. Mechanical and histologic changes in canine vein grafts. J Surg Res. 1988;44(3):259-65.

[9] Ellozy SH, Carroccio A, Minor M, Jacobs T, Chae K, Cha A et al. Challenges of endovascular tube graft repair of thoracic aortic aneurysm: Midterm follow-up and lessons

learned. J Vasc Surg. 2003;38(4):676-83.

[10]Ethier CR, Simmons CA. Introductory biomechanics: From cells to organisms. Cambridge texts in biomedical engineering. Cambridge: Cambridge University Press; 2007.

[11]Fung Y-C. Biomechanics: Mechanical properties of living tissues. Second ed. Springer; 1993.

[12]Gamble JR, Matthias LJ, Meyer G, Kaur P, Russ G, Faull R et al. Regulation of in vitro capillary tube formation by anti-integrin antibodies. J Cell Biol. 1993;121(4):931-43.

[13]Gorman SP, Jones DS, Bonner MC, Akay M, Keane PF. Mechanical performance of polyurethane ureteral stents in vitro and ex vivo. Biomaterials. 1997;18(20):1379-83.

[14]Grapski JA, Cooper SL. Synthesis and characterization of non-leaching biocidal polyurethanes. Biomaterials. 2001;22(16):2239-46.

[15]Holzapfel GA, Gasser TC, Ogden RW. A new constitutive framework for arterial wall mechanics and a comparative study of material models. J Elasticity. 2000;61(1-3):1-48.

[16]Info sheet no. 4: Selected properties of NiTi. Memory-Metalle GmbH, Weil am Rhein. 2006. http://www.memory-metalle.de/html/03_knowhow/PDF/MM_04_properties_e.pdf. Accessed 29/04/2010.

[17]Jacobs TS, Won J, Gravereaux EC, Faries PL, Morrissey N, Teodorescu VJ et al. Mechanical failure of prosthetic human implants: A 10-year experience with aortic stent graft devices. J Vasc Surg. 2003;37(1):16-26.

[18]Kim JH, Kang TJ, Yu W-R. Mechanical modeling of self-expandable stent fabricated using braiding technology. J Biomech. 2008;41(15):3202-12.

[19]Kleinstreuer C, Li Z, Basciano CA, Seelecke S, Farber MA. Computational mechanics of Nitinol stent grafts. J Biomech. 2008;41(11):2370-8.

[20]Konnerth J, Gindl W, Müller U. Elastic properties of adhesive polymers. I. Polymer films by means of electronic speckle pattern interferometry. J Appl Polym Sci. 2007;103(6):3936-

9.

[21]Levy B, Tedgui A, editors. Biology of the arterial wall. Dordrecht: Kluwer; 1999.

[22]Mailhot B, Komvopoulos K, Ward B, Tian Y, Somorjai GA. Mechanical and friction properties of thermoplastic polyurethanes determined by scanning force microscopy. J Appl Phys. 2001;89(10):5712-9.

[23]Min HK, Lee YT, Kim WS, Yang JH, Sung K, Jun TG et al. Complete revascularization using a patent left internal thoracic artery and variable arterial grafts in multivessel coronary reoperation. Heart Surg Forum. 2009;12(5):244-9.

[24]Mooney DJ, Baldwin DF, Suh NP, Vacanti JP, Langer R. Novel approach to fabricate porous sponges of poly(-lactic-co-glycolic acid) without the use of organic solvents. Biomaterials. 1996;17(14):1417-22.

[25]Mortier P, Holzapfel G, De Beule M, Van Loo D, Taeymans Y, Segers P et al. A novel simulation strategy for stent insertion and deployment in curved coronary bifurcations: Comparison of three drug-eluting stents. Ann Biomed Eng. 2010;38(1):88-99.

[26]Newman Dorland WA. Dorland's illustrated medical dictionary. 29 ed. Philadelphia: Saunders; 2000.

[27]Peynircioglu B, Ergun O, Hazirolan T, Serter T, Ucar I, Cil B et al. Stent-graft applications in peripheral non-atherosclerotic arterial lesions. Diagn Interv Radiol. 2008;14(1):40-50.

[28]Sakai H, Urasawa K, Oyama N, Kitabatake A. Successful covering of a hepatic artery aneurysm with a coronary stent graft. Cardiovasc Intervent Radiol. 2004;27(3):274-7.

[29]Tai NR, Salacinski HJ, Edwards A, Hamilton G, Seifalian AM. Compliance properties of conduits used in vascular reconstruction. Br J Surg. 2000;87(11):1516-24.

[30]van der Merwe H, Daya Reddy B, Zilla P, Bezuidenhout D, Franz T. A computational study of knitted Nitinol meshes for their prospective use as external vein reinforcement. J Biomech. 2008;41(6):1302-9.

[31]Wiggins MJ, Anderson JM, Hiltner A. Biodegradation of polyurethane under fatigue loading. J Biomed Mater Res, Part A. 2003;65A(4):524-35.

[32]Wong G, Li J-m, Hendricks G, Eslami MH, Rohrer MJ, Cutler BS. Inhibition of experimental neointimal hyperplasia by recombinant human thrombomodulin coated ePTFE stent grafts. J Vasc Surg. 2008;47(3):608-15.

[33]Xu W, Zhou F, Ouyang C, Ye W, Yao M, Xu B. Mechanical properties of small-diameter polyurethane vascular grafts reinforced by weft-knitted tubular fabric. J Biomed Mater Res, Part A. 2010;92A(1):1-8.

[34]Yeoman MS. The design and optimisation of fabric reinforced porous prosthetic grafts using finite element methods and genetic algorithms [Phd]. Cape Town: University of Cape Town; 2004.

[35]Yeoman MS, Reddy BD, Bowles HC, Zilla P, Bezuidenhout D, Franz T. The use of finite element methods and genetic algorithms in search of an optimal fabric reinforced porous graft system. Ann Biomed Eng. 2009;37(11):2266-87.

[36]Zilla P, Bezuidenhout D, Human P. Prosthetic vascular grafts: Wrong models, wrong questions and no healing. Biomaterials. 2007;28(34):5009-27.

[37]Zilla P, Human P, Wolf M, Lichtenberg W, Rafiee N, Bezuidenhout D et al. Constrictive external nitinol meshes inhibit vein graft intimal hyperplasia in nonhuman primates. J Thorac Cardiovasc Surg. 2008;136(3):717-25.

[38]Zilla P, Wolf M, Rafiee N, Moodley L, Bezuidenhout D, Black M et al. Utilization of shape memory in external vein-graft meshes allows extreme diameter constriction for suppressing intimal hyperplasia: A non-human primate study. J Vasc Surg. 2009;49(6):1532-42.

TABLES

Table 1. PPU material parameters[35] used in the hyperfoam material model.

Description	Unit	Value
υ	-	0.035
μ_1	MPa	0.19262
μ_2	MPa	-0.03373
μ_3	MPa	-0.08682
μ_4	MPa	0.02566
α_1	-	1.2571
α_2	-	1.2655
α_3	-	-2.6509
α_4	-	-4.6589

Table 2. Nitinol material parameters[30] used in the shape memory alloy user material.

Parameter	Unit	Value
Austenite Young's Modulus	MPa	38992
Austenite Poisson's Ratio	-	0.46
Martensite Young's Modulus	MPa	21910
Martensite Poisson's Ratio	-	0.46
Transformation Strain	-	0.042
Loading Temperature Derivative of Stress	MPa/°C	0
Loading Start of Transformation Stress	MPa	483
Loading End of Transformation Stress	MPa	610
Reference Temperature	MPa	37
Unloading Temperature Derivative of Stress	MPa/°C	0
Unloading Start of Transformation Stress	MPa	388
Unloading End of Transformation Stress	MPa	256
Loading Start of Transformation Stress (Compression)	MPa	610
Volumetric Transformation Strain	-	0.04
Number of Annealings to be Performed During Analysis	-	0

Table 3. Maximum principal stress σ (in MPa) and strain ε (in %) in the PPU scaffold and the reinforcement mesh at 80, 120 and 200 mmHg. For non-reinforced models, the mesh was not applicable.

| | 80 mmHg | | | | 120 mmHg | | | | 200 mmHg | | | |
| | PPU | | Mesh | | PPU | | Mesh | | PPU | | Mesh | |
	σ	ε	σ	ε	σ	ε	σ	ε	σ	ε	σ	ε
NIEX	0.020	8.94	73.68	0.20	0.031	12.77	97.0	0.27	0.046	17.25	157.90	0.43
PUEX	0.036	15.43	18.76	3.44	0.054	21.41	28.18	5.01	0.063[a]	24.32[a]	33.61[a]	5.96[a]
BG2.4	0.066	27.53	-	-	0.132	50.28	-	-	2.54[b]	192.7[b]	-	-
NIEM	0.012	5.72	57.59	0.09	0.019	7.46	86.72	0.14	0.034	13.83	145.60	0.24
PUEM	0.37	16.25	18.16	2.99	0.055	22.54	26.64	4.42	0.095	32.75	45.14	7.15
BG2.8	0.081	33.41	-	-	0.186	68.47	-	-	2.49[c]	192.4[c]	-	-

[a] predicted at 143 mmHg; [b] predicted at 170 mmHg; [c] predicted at 150 mmHg
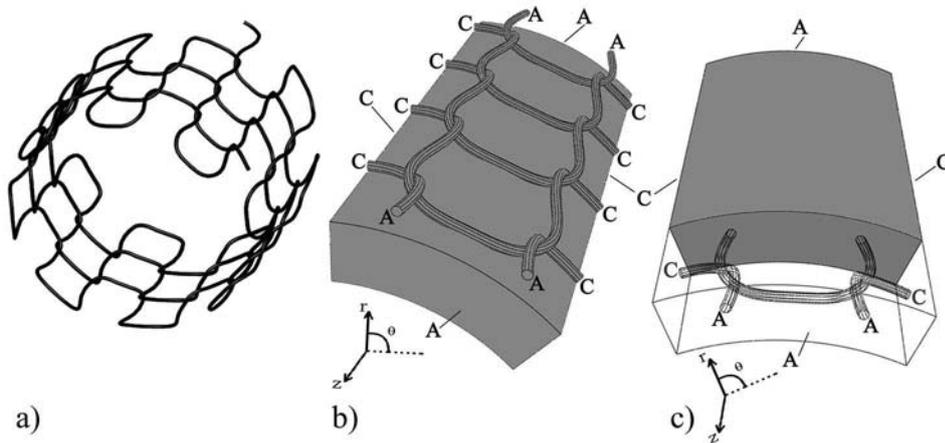
Figure 1. Computational 3D geometry of the knitted wire mesh (a). A partially geometry of the knitted mesh created from single loop geometry was combined with a 45º circumferential section of the tubular PPU scaffold to obtain an externally reinforced graft (b) and a graft with embedded reinforcement (c). Labels A and C indicate surfaces that obtained axial and circumferential boundary conditions, respectively.
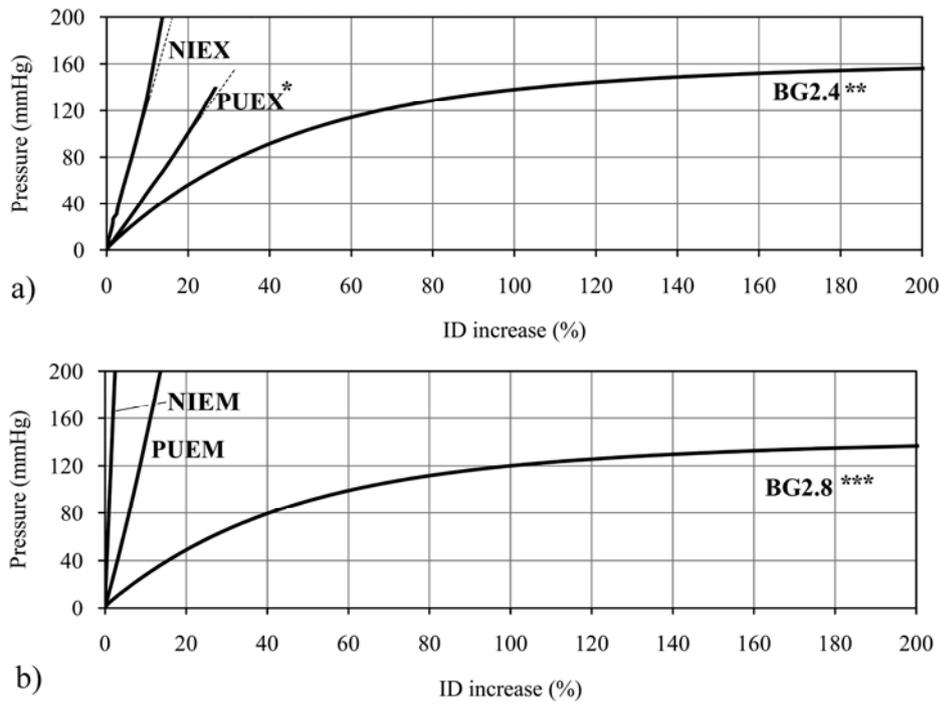
Figure 2. Graphs illustrating the relationship of pressure and diameter increase for different graft models. The increase in ID was normalized to the initial ID at zero pressure. a) Externally reinforced grafts (Nitinol mesh: NIEX, PU mesh: PUEX; *termination at 143 mmHg) and associated non-reinforced scaffold (BG2.4, **termination at 170 mmHg). The dashed straight lines were added to enhance the illustration of increase in slope of the NIEX and PUEX curves. b) Grafts with embedded reinforcement (Nitinol mesh: NIEM, PU mesh: PUEM) and the associated non-reinforced scaffold (BG2.8, ***termination at 150 mmHg).
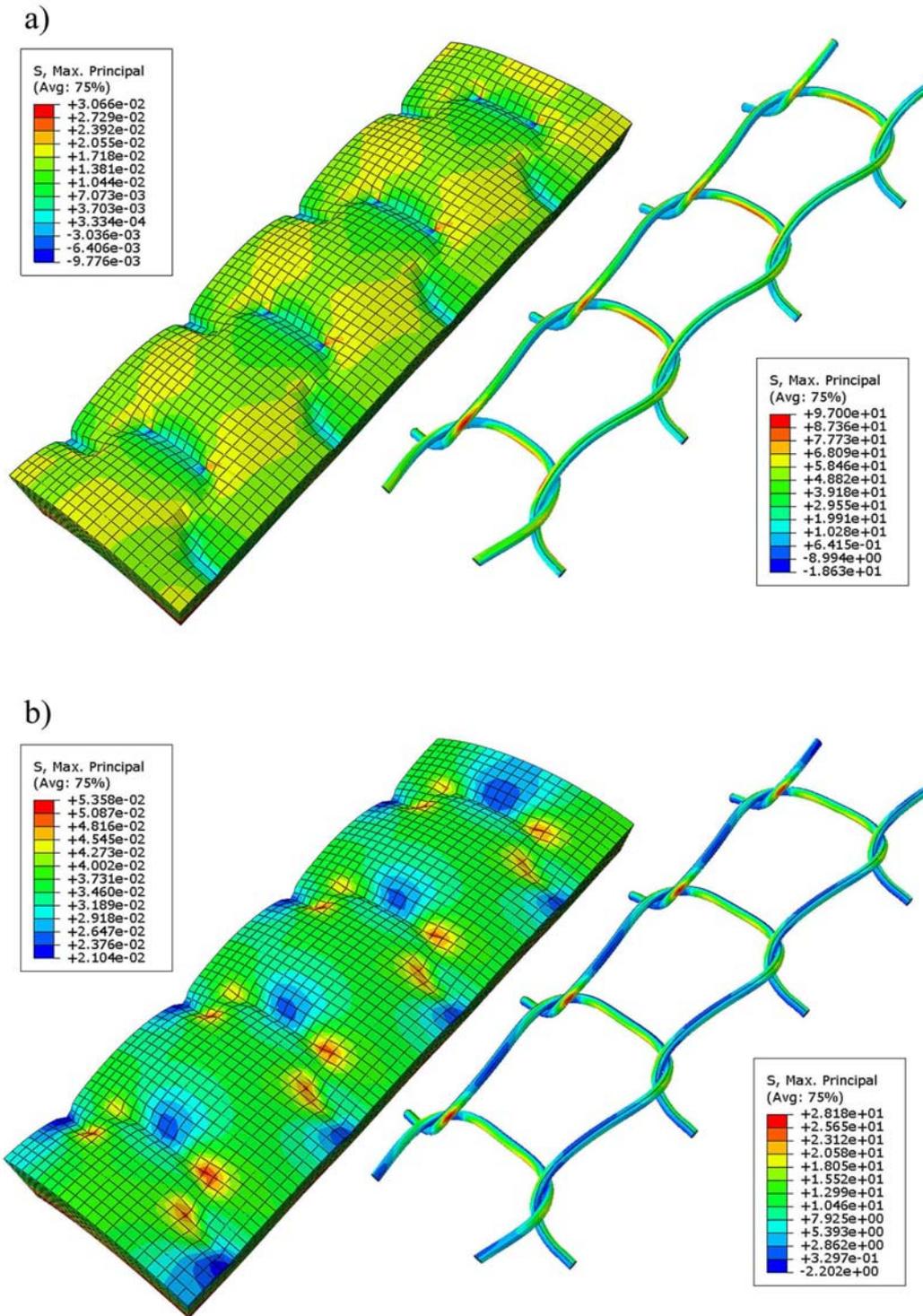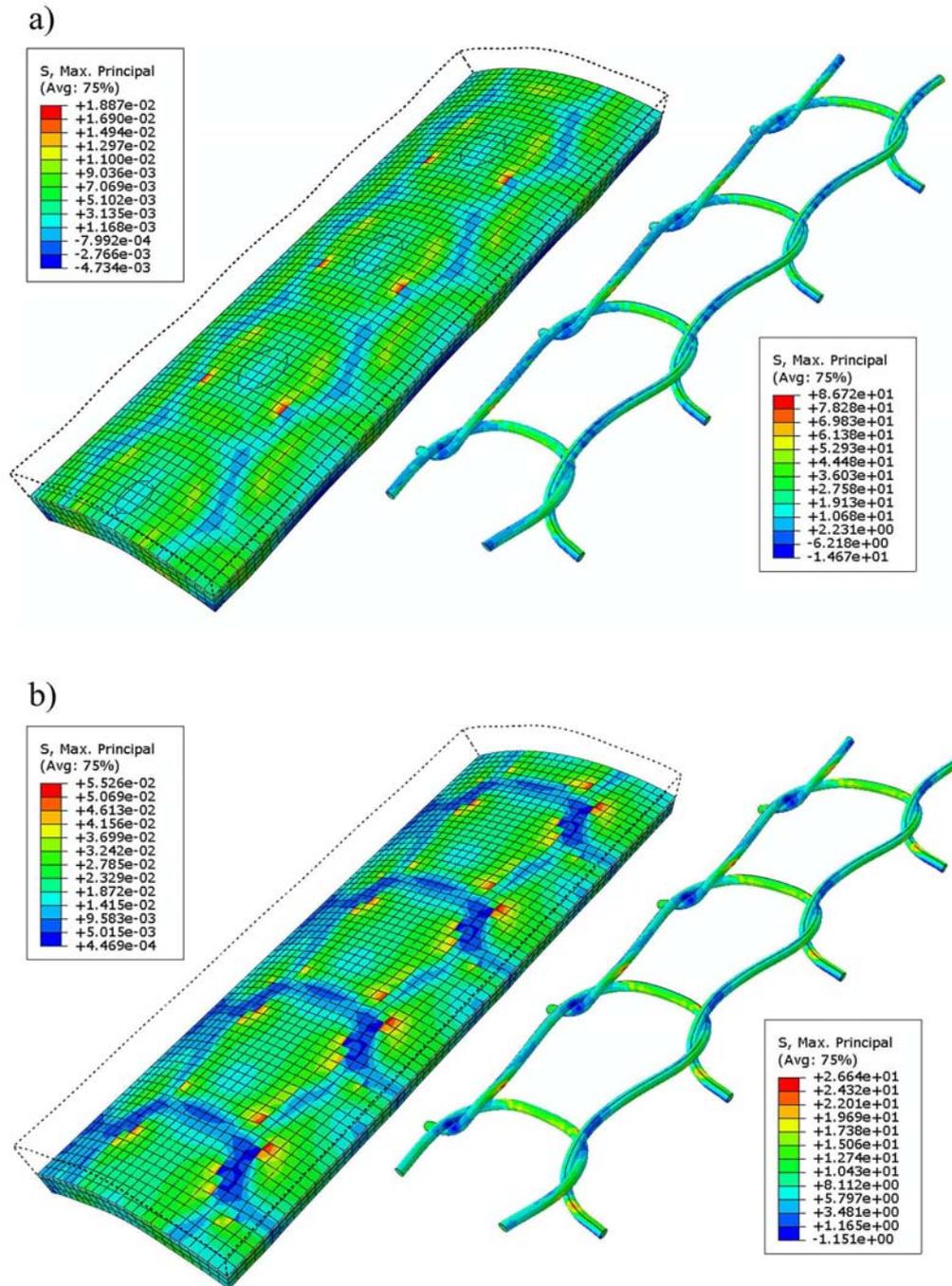
Figure 3. Contour plots of the distribution of the maximum principal stress (values in MPa) at 120 mmHg in the deformed PPU scaffold and the wire mesh of the externally reinforced model for a) Nitinol wire mesh (NIEX) and b) PU wire mesh (PUEX). The wire mesh was detached from the PPU scaffolds and assigned separate legends for display purposes. In each model, stress concentrations were predicted on the abluminal surface of the PPU scaffold and in the heads and at intersections of wire loops.

Figure 4. Contour plots of the distribution of the maximum principal stress (values in MPa) at 120 mmHg in the deformed PPU scaffold and the wire mesh of model with embedded reinforcement with a) Nitinol wire mesh (NIEM) and b) PU wire mesh (PUEM). The wire meshes were detached from the PPU scaffolds and assigned separate legends for display purposes. In each model, stress concentrations were predicted in the internal elements of the PPU scaffold and in the heads and crossovers of wire loops. For the PPU scaffold, abluminal layers of elements were eliminated from the display to reveal the locations of stress concentration.
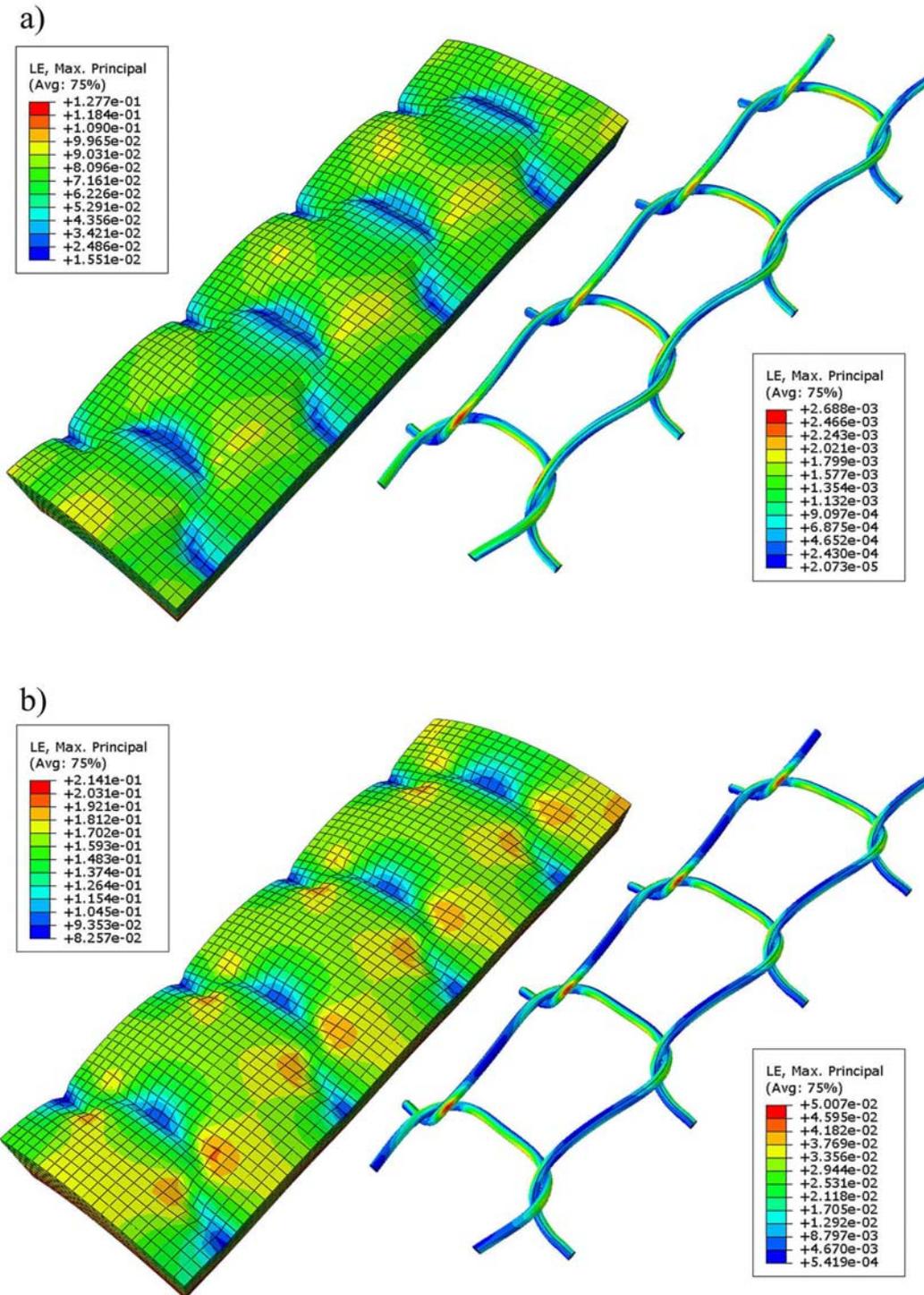
Figure 5. Contour plots of the distribution of the maximum principal strain (values in %) at 120 mmHg in the deformed PPU scaffold and the wire mesh of the externally reinforced model for a) Nitinol wire mesh (NIEX) and b) PU wire mesh (PUEX). The wire mesh was detached from the PPU scaffold and assigned separate legends for display purposes. In each model, strain concentrations were predicted on the abluminal surface of the PPU scaffold and in the heads and at intersections of wire loops.
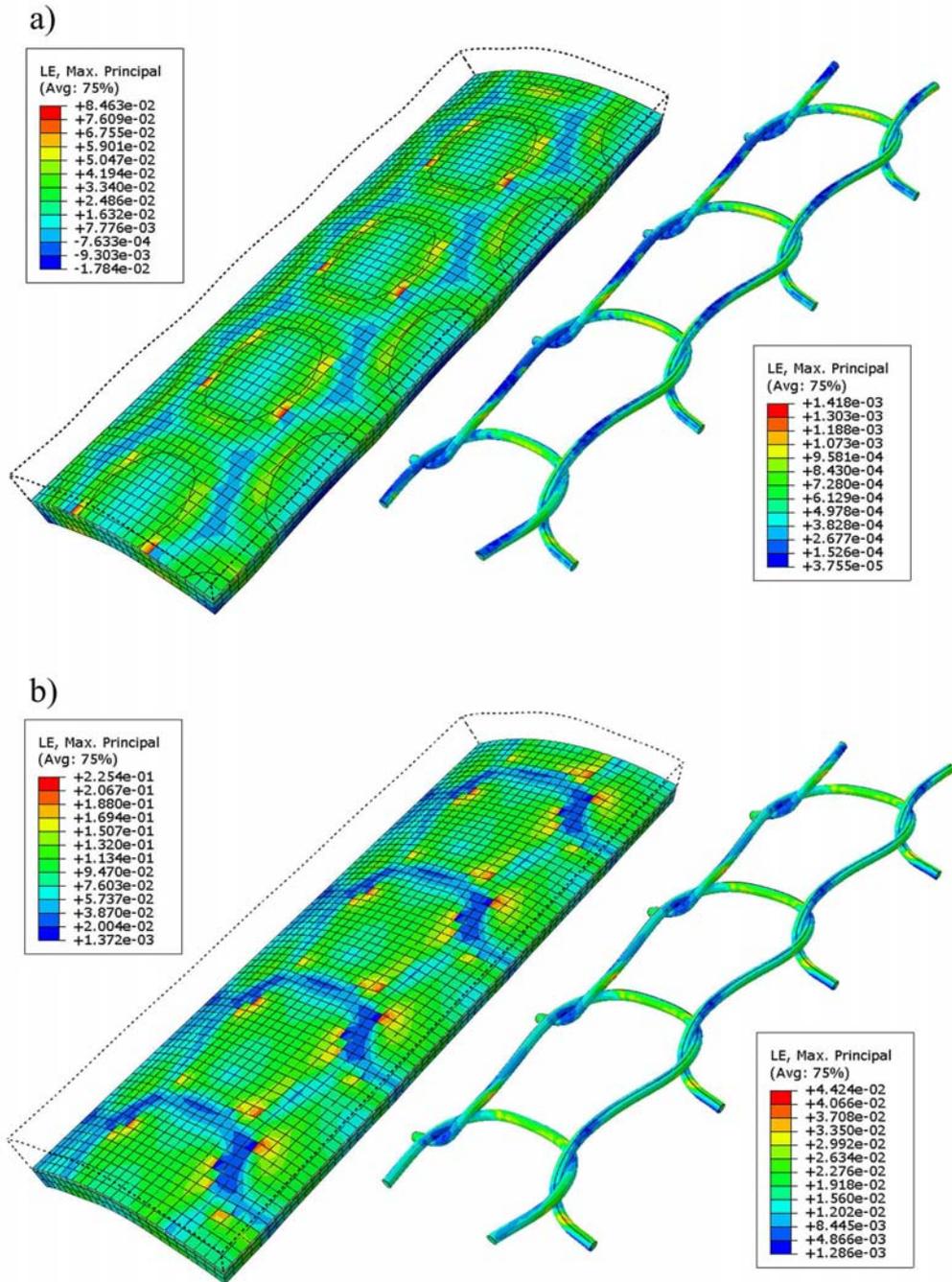
Figure 6. Contour plots of the distribution of the maximum principal strain (values in %) at 120 mmHg in the deformed PPU scaffold and the wire mesh of model with embedded reinforcement with a) Nitinol wire mesh (NIEM) and b) PU wire mesh (PUEM). The wire mesh was detached from the PPU scaffold and assigned separate legends for display purposes. In each model, strain concentrations were predicted in the internal elements of the PPU scaffold and in the heads and crossovers of wire loops. For the PPU scaffold, abluminal layers of elements were eliminated from the display to reveal the locations of strain concentration.
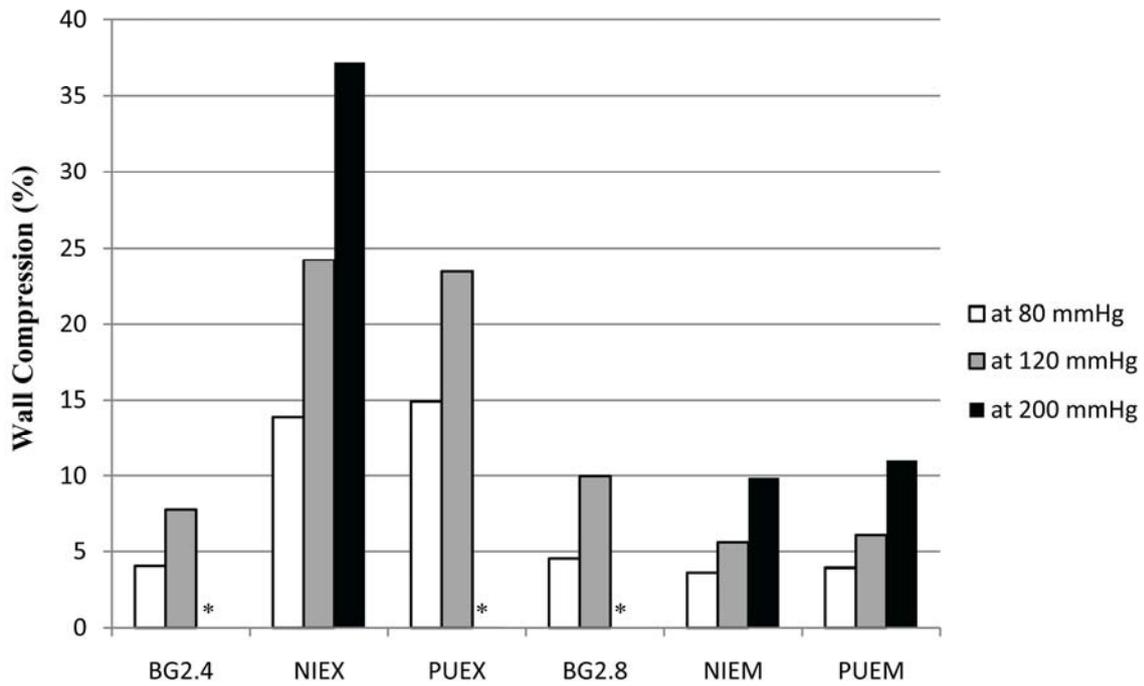
Figure 7. Wall compression predicted by the six models at 80, 120 and 200 mmHg. (*: The PUEX, BG2.4 and BG2.8 models terminated at 143, 170 and 150 mmHg, respectively). A considerable increase in wall compression was observed for models with external reinforcement (NIEX and PUEX) compared to the associated non-reinforced model (BG2.4). The models with embedded reinforcement (NIEM and PUEM), exhibited lower wall compression compared to the non-reinforced model (BG2.8).